JOURNAL OF MATERIALS SCIENCE **40** (2005) 1749–1755

# Modeling mechanical responses in a laminated biocomposite

## Part II *Nonlinear responses and nuances of nanostructure*

K. KATTI*, D. R. KATTI, J. TANG, S. PRADHAN
*Department of Civil Engineering, CIE 201, North Dakota State University, Fargo, ND 58105, USA*
*E-mail: Kalpana.Katti@ndsu.nodak.edu*

M. SARIKAYA
*Department of Materials Science and Engineering, University of Washington, Box 352120, Seattle, WA 98195, USA*

Accurate pseudo-hexagonal nanoarchitecture of nacre was used to design three dimensional finite element models of nacre, the inner layer of mollusk shells. Tensile tests were simulated introducing linear and nonlinear material properties in these models. Material parameters of components of nacre (aragonitic bricks and the complex organic phase) such as elastic modulus and hardness were obtained from bulk measurements reported in literature. In addition, nanoscale experiments conducted using atomic force microscopy and nanoindentation provided mechanical properties of aragonite platelets and organic phase. Linear simulations in the elastic regime at low stresses (2 MPa) was conducted on the new models. Our simulations indicate that a high modulus of organic phase (∼20 GPa) is necessary to obtain the experimentally obtained bulk phase elastic response of nacre. Our nanoindentation experiments also confirmed the simulations. Further nonlinear simulations were conducted under the assumption of a fully elastic behavior of aragonite and an elastoplastic model for the organic phase. Further the yield stress of the organic phase is varied over a wide range from 40 to 400 MPa . The resulting yield stress of nacre was compared to experimentally obtained value. Again our simulations indicate that an exceptionally high yield stress of the organic phase is necessary to obtain the yield behavior in nacre. Further, nanostructural nuances in the form of platelet-platelet mineral contacts were incorporated in the three dimensional models. The role of these mineral contacts on linear and nonlinear responses under high and low loads was quantitatively evaluated. Our simulations indicate for the first time that presence of these mineral contacts has minimal effect on both linear and nonlinear responses in nacre. As a matter of fact, the contacts are regions of high stress concentration and they break long before yield begins in nacre (∼50 MPa). These results have significant ramifications on a biomimetic design of scalable nanocomposites mimicking nacre.


### 1. Introduction

The exceptional mechanical response of nacre, the inner layer of seashells, to external loading, is extensively studied in literature [1–6]. Due to the exceptional properties of fracture toughness and strength, it represents a model system for biomimetic design [7–11]. Nacre is ceramic laminated composite consisting of highly organized polygonal shaped aragonitic platelet layers of thickness of 0.5 $\mu$m separated by thin 30 nm layers of organic composed mainly of proteins and polysaccharides. This laminated 'brick and mortar' microarchitecture is responsible for the high strength and fracture toughness of nacre. The portion of the nacre comprising the organic material typically represents 1 to 5% by weight. Microstructural characterization has shown the presence of a highly hierarchical morphology i.e., architectural order at many length scales, from nm to mm, not found in man-made systems [2, 7]. The aragonitic structure also occurs in deposits of geologic origin and exhibits identical crystallographic structure but small differences are detected in the electronic structure possibly from the influence of organic [12].

*Author to whom all correspondence should be addressed.

Often the true physical continuum of the macroscopic structures is discretized into smaller sections using numerical modeling techniques such as finite element modeling [13]. Many engineered structures are designed and modeled using numerical modeling techniques. Finite element modeling is a commonly used tool for design of structures as diverse as buildings, bridges, roads, aircrafts, automobiles, artificial hard and soft tissues etc. This is particularly true for modeling mechanical response of biological soft and hard tissues [14–16]. In our previous work [17–19], we constructed the microarchitecture of nacre using three dimensional finite element modeling techniques. Material parameters for organic and inorganic phases were obtained from atomic force microscopy and nanoindentation experiments in literature. Simulated tensile tests were conducted at low and high loads to predict linear and nonlinear properties of the 'composite'. Our previous models are expanded in this work to represent more accurately the micro and nanoarchitecture of nacre. In addition, novel methods (as described in part I) are used to obtain nanoscale mechanical responses in individual components of nacre.

## 2. Formulation of finite element model of nacre

In our previous work [17], we designed 3D finite element models of nacre using FEM software, MARC$^{TM}$ (MSC MARC Corp.) on a Silicon Graphics workstation along with a pre and post processor, MENTAT$^{TM}$ (MSC MARC Corp.). These models were constructed based on a simplistic brick and mortar architecture. In the current work, the true (pseudo) hexagonal symmetry of nacre platelets is incorporated into the construction of the models. In addition, some structural nuances such as presence of thin mineral contacts through the aragonitic platelets is also included. In the present work a four processor SUN ES 3500 workstation at NDSU and ORIGIN 2000 massively parallel supercomputer at National Center for Supercomputing Applications (NCSA) has been used along with pre and post processor, MENTAT$^{TM}$ (MSC MARC Corp.). The details of the construction of the model are as follows.

### 2.1. Construction of the 3D model

The construction of the model was done in three phases (1) building of the individual unit, (2) building of a block comprising of two units rotated, stacked and connected to one another (Fig. 1a) and (3) building of the 10 $\times$ 10 $\times$ 8 model (shown in Fig. 2) through rotating and translating of the two unit blocks. A four noded plain isoparametric element was chosen and a equilateral triangular element with sides 2.5 $\mu$m long is constructed. The triangular element is subdivided to form an equilateral triangular four noded isoparametric element with sides 0.025 $\mu$m (25 nm) long. This smaller triangular element will be part of the hexagonal connection for contact. A node is next introduced at the base edge of the larger triangular element with coordinates of $-(2.5 * \sin(60^\circ) * \tan(25^\circ)$ and $-2.5 * \sin(60^\circ)$. An additional element is then introduced within the larger triangular element with the new node as part of the element. This new node along with the nodes in the central region of the larger triangular element provide for connectivity to adjacent lower unit. Material properties for aragonite are assigned to the elements. Next, a 10 nm thick 4-noded isoparametric element is attached to the base of the larger triangular element and assigned properties for organic material. This forms the basic triangular plane for construction of the 3D unit. The triangular plane is next expanded vertically through a distance of 0.25 $\mu$m to form one sixth of 3D hexagonal aragonite platelet. The same plane is expanded 10 nm above and below the aragonite platelet to form the 10 nm thick organic layer on the aragonite platelet. The contact elements near the vertex are assigned aragonite properties. These elements now form one sixth of the 3D hexagonal aragonite contact. The surface contact nodes are rotated through 5 degrees to provide connectivity with the rotated unit above. The expanded elements

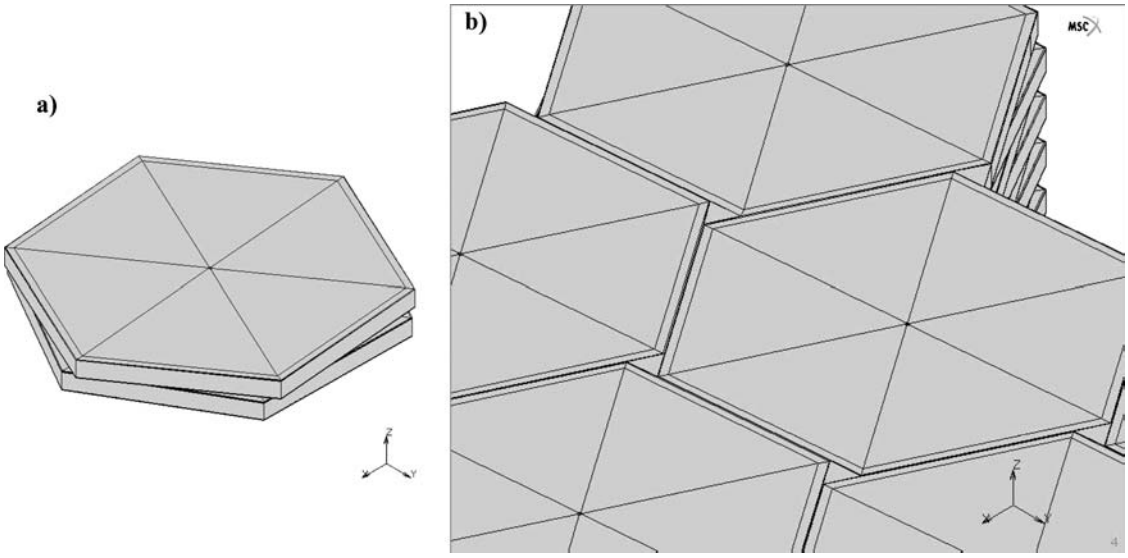


*Figure 1* (a) Figure showing two individual units of 5 $\mu$m diameter 0.25 $\mu$m high hexagonal aragonite platelets covered with 10 nm thick organic layer. The individual units are rotated with respect to one another by an angle of 5 degrees. The 50 nm contacts are located at the center. Each unit consists of 72 eight noded 3D isoparametric elements. (b) Figure showing a close up view of three-dimensional stacking of the individual units.

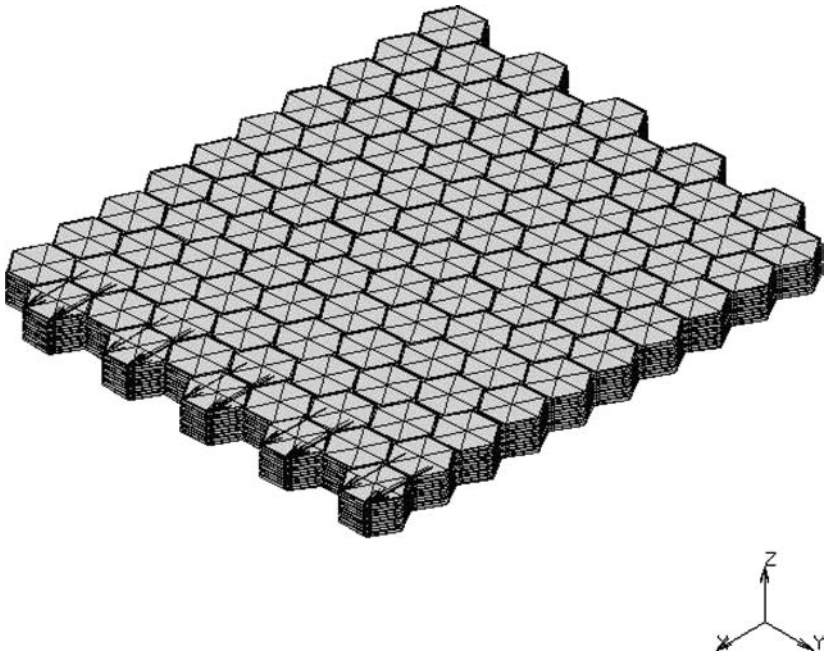


*Figure 2* Figure showing the three-dimensional model comprising of 10 × 10 × 8 high stacked units.

automatically become 3D 8-noded isoparametric elements. The 3D subunit containing one sixth of the inorganic platelet, organic cover and contact is next translated vertically through 0.27 $\mu$m and rotated 5 degrees to form the subunit of the upper unit. Next, all elements are rotated and duplicated five times to form the dual unit stacked block seen in Fig. 1a. The block is then rotated along the vertical axis through 30 degrees. A close up view of three-dimensional stacking of the individual units is shown in Fig. 1b. After the dual unit block is constructed, the block is translated and duplicated nine times to form a row of 10 blocks. The row is then translated and duplicated to form a sheet of 10 × 10 blocks. Due to relative rotation between the upper and lower units, minute triangular voids are formed at the intersection of three blocks. These voids were filled by a three layered triangular block having the same thickness of the inorganic and organic layers as in the individual units. The sheet is then translated and duplicated 4 times vertically to form a block of 10 × 10 × 8 as shown in Fig. 2. All FEM simulations were conducted on this 10 × 10 × 8 block. A close-up view of a section through the individual units to show the contacts between platelets is shown in Fig. 3. The

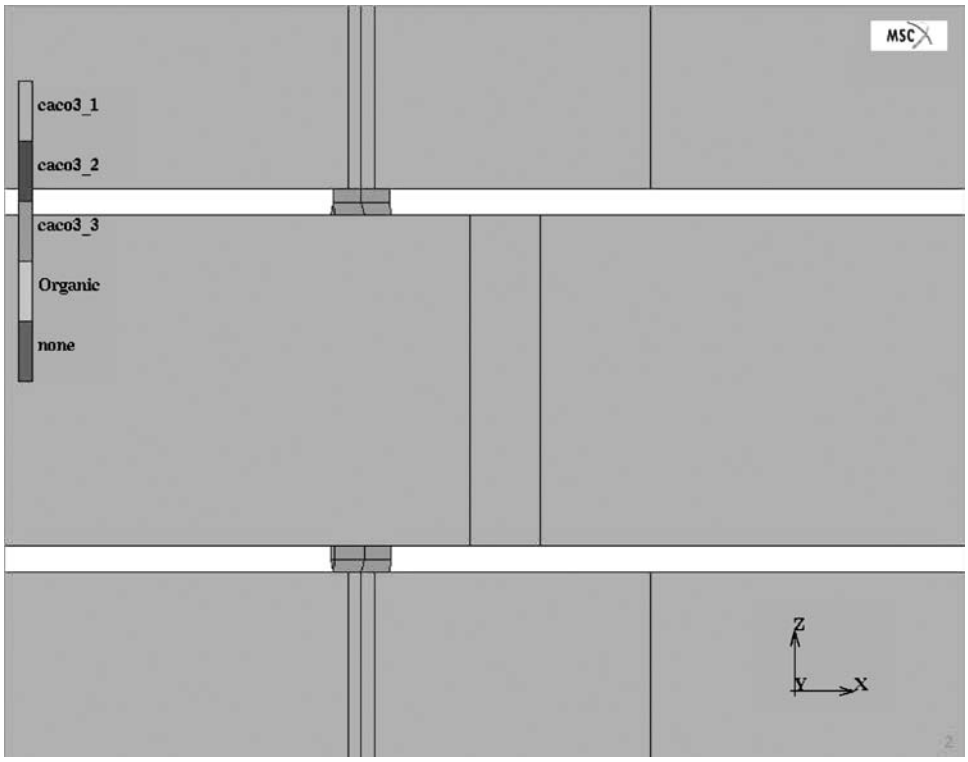


*Figure 3* Close up view of a section through the individual units to show the contacts between platelets. The organic layer between the aragonite platelets has been removed to show the contacts clearly.

organic layer between the aragonite platelets has been removed to show the contacts clearly.

For conducting simulated tensile and compressive tests, the organic layer on the bottom of the block was removed and "glued" by assigning zero nodal displacements. The organic layer from the top surface was also removed and uniform normal stress was applied to the element faces. To reduce edge effect, the edge nodes were tied to the central nodes during testing.

## 2.2. Determination of nanoscale mechanical properties of biocomposite nacre

Material parameters for the different sections in our models were obtained using nanomechanical tests using atomic force microscopy. Details of these experiments are described in our previous work [18]. Elastic modulus and hardness of the aragonite platelets as well as the organic matrix were obtained using ultrafine indentations provided by the atomic force microscopy

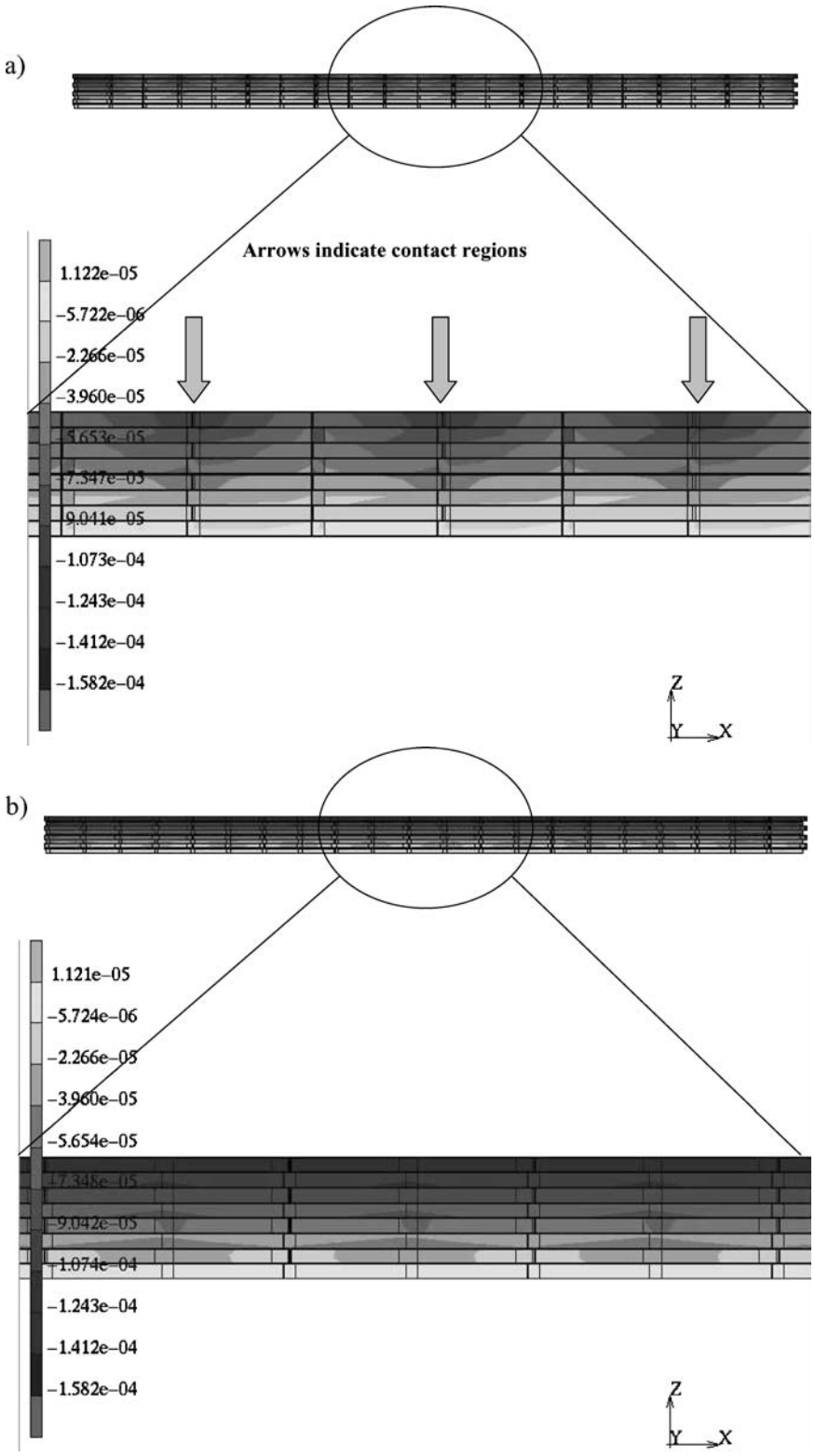


*Figure 4* Figure showing the distribution of normal stress in the central region of the model: (a) with contacts and (b) without contacts. The influence of contacts is seen by local stress concentration in the contact regions. Load = 2 MPa.

TABLE I Material parameters of constituents of nacre

| | Nacre-aragonite | Geological aragonite | Organic |
|---|---|---|---|
| $E$ (GPa) | 80 | 100 | 20 |
| $H$ (GPa) | 4.3 | 7.0 | [a] |

[a]Not determined.

techniques. Vertical indentations were performed using a Hysitron Picoindentation™ system that is attached to an atomic force microscope (AFM) (Park CP Scanning probe System). The methodology for determining nanoscale $E$ and $H$ values using the setup are well documented [20]. Material parameters of the organic and inorganic phases are shown in Table I.

## 2.3. Boundary conditions

Tensile and compression tests were simulated by setting nodal displacements of the lowest face of the 3D model to zero and applying face pressure in the $z$ direction to the top face of the 3D model. These boundary conditions were applied directly to aragonite surfaces. As before, all the nodal displacements on the top aragonite face were equalized by linking all surface nodes to central node which effectively minimizes the 'edge effect' commonly observed in FEM analyses.

## 3. Results and discussion

Initially, tensile tests were conducted with single load increment of $2 \times 10^{-6}$ N/$\mu$m$^2$ (2 MPa) on the new 3D model. The property of elements in the contacts was maintained at two values, aragonitic like and organic like. Simulations were conducted for these two extreme cases. This is identical to running simulations for models with and without contacts respectively. The resulting displacements of elements are shown in Fig. 4 a and b for the two cases. In these Figs a section of the simulation through the $x$-$z$ plane is shown. As seen, clearly, in the contacts-present models, localized displacement variations are observed in the regions of mineral contacts. For the contacts-absent models such localized displacements are not seen. For the $10\times10\times8$ unit system, the net displacement in the z direction for the contacts-absent model was observed to be $1.34 \times 10^{-4}$ $\mu$m which corresponds to an elastic modulus of nacre to be 31.9 GPa. Results of identical simulations on contacts-present and the contacts-absent models are shown in Table II. As seen, the calculated modulus in the two cases are only marginally different. Similar simulations were conducted at higher loads upto $60 \times 10^{-6}$ N/$\mu$m$^2$(60 MPa). Sections through simulations of the contacts-present models showing displacements in $z$ direction for single load increment of $9.25 \times 10^{-6}$ N/$\mu$m$^2$ (9.25 MPa) are shown in Fig. 5. Again significant

TABLE II Elastic Modulus of nacre with and without contacts under single load increment of 2 MPa

| | Deformation in $z$ direction ($\mu$m) | Strain | $E$ (GPa) |
|---|---|---|---|
| Contacts | 1.3400E-04 | 6.3208E-05 | 31.6416 |
| No contacts | 1.3428E-04 | 6.3396E-05 | 31.5477 |

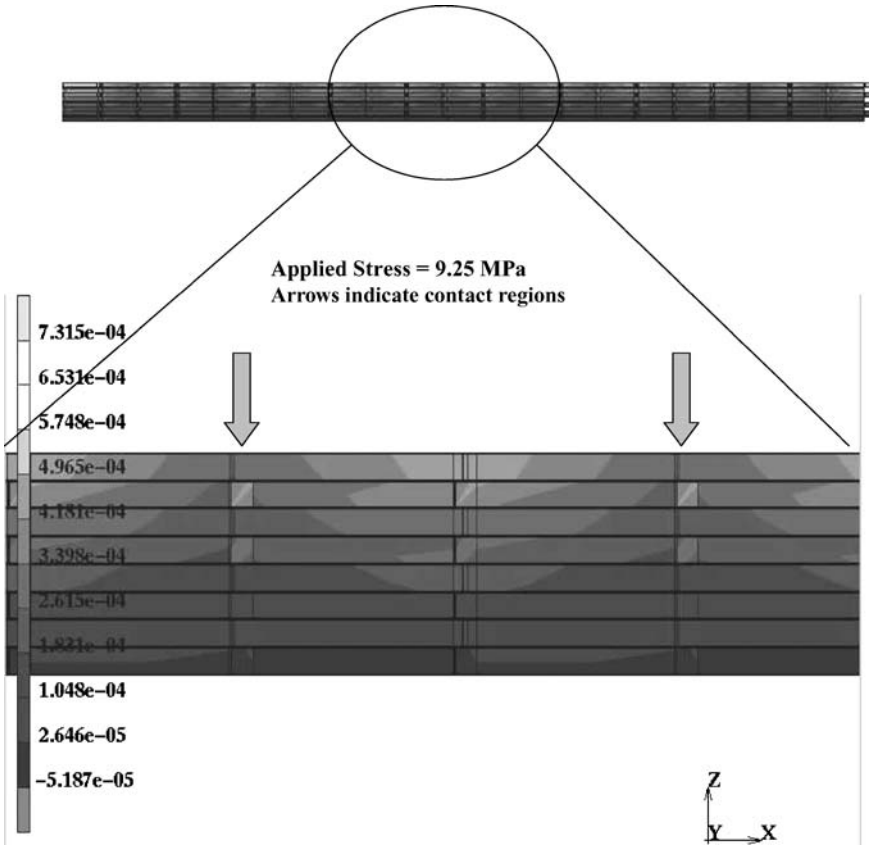


*Figure 5* Figure showing the distribution of normal stress in the central region of the model with contacts. The influence of contacts is seen by local stress concentration in the contact regions. Load = 9.25 MPa.

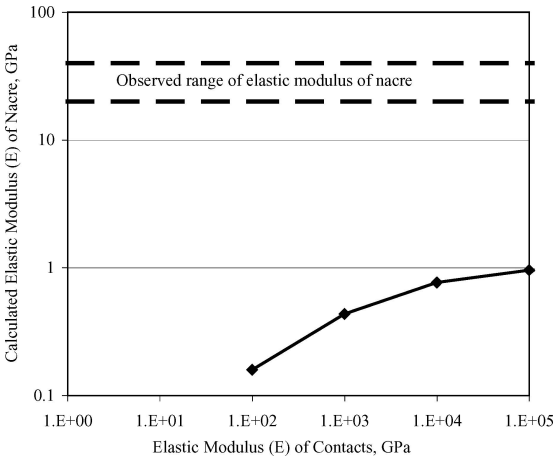


*Figure 6* Results of parametric study using the model showing that increasing elastic modulus of inorganic contacts by even several orders of magnitude does not bring the calculated elastic modulus of nacre to that observed. These results further indicate that the contacts have negligible effect on the elastic modulus of nacre.

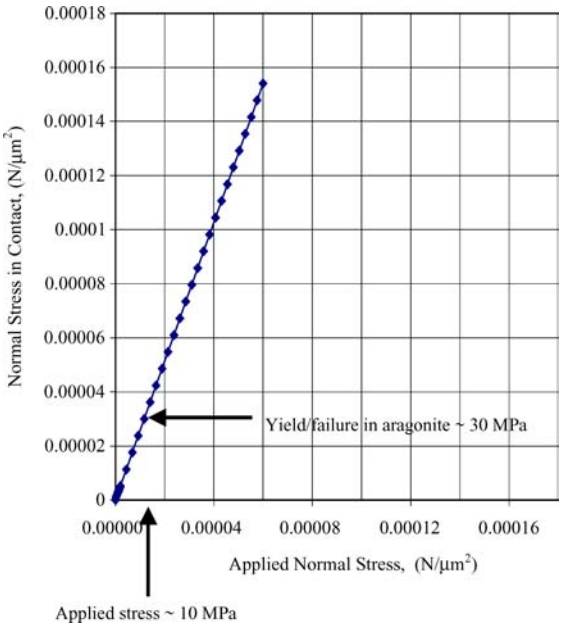


*Figure 7* Plot of applied normal stress versus normal stress in contacts. The normal stress in contacts is about 3 times larger than the applied stress. The contacts yield at an applied normal stress level of about 10 MPa, which is much smaller than the observed yield stress of nacre of about 50 MPa. The contacts have no influence on the yielding behavior of nacre.

variations in displacements near contact regions is observed as compared to the contacts-absent samples.

Since our previous work [18] has indicated both through simulations and nanoindentation experiments that the organic phase is indeed a material of extremely high elastic modulus (∼20 GPa), we extend our simulations for the current hexagonal symmetry models. In order to accomplish this, a previously postulated low modulus of organic phase (5 MPa) was applied to the material properties of the organic phase in our 3D model. Further, the elastic modulus of the contact regions was varied from 10 GPa to extremely high values of 100,000 GPa. Simulations at single load increment of $2 \times 10^{-6}$ N/$\mu$m$^2$ (2 MPa) for each of these cases were performed. Fig. 6 shows the calculated elastic modulus for varying values of modulus of the contacts regions. The dotted line at the top of the Fig. indicated the experimentally observed elastic modulus of nacre. As seen, extremely large values of modulus of the organic phase are necessary to result in the experimentally obtained elastic behavior of nacre.

Since our simulations suggest that the elastic response of nacre is only marginally affected by the presence of contacts, we wish to further investigate the influence of contacts on the yield behavior in nacre. The effective stress in the contact regions was obtained from the above simulations for low and high loads. The effective stress in the contact regions was plotted against the applied stress in nacre as shown in Fig. 7. Clearly, the effective stress in the contact region is higher than that applied. Since aragonite yields at ∼30 MPa the applied stress at which this yield condition results in the contact regions is at ∼10 MPa.

We also studied the influence of yield stress of individual components (organic and aragonite) on the yielding of nacre. Our previous work [18] has shown that the yield stress of the organic phase in nacre is extremely high (∼400 MPa) compared to the magnitude of yield stress of common organic materials such as proteins obtained from bulk mechanical tests. We evaluated the response of nacre using the nonlinear material model described above for a range of values of yield stress of organic phase keeping the yield stress of aragonite constant. The results from the simulations are shown in Fig. 8. In the first set of simulations, the yield stress

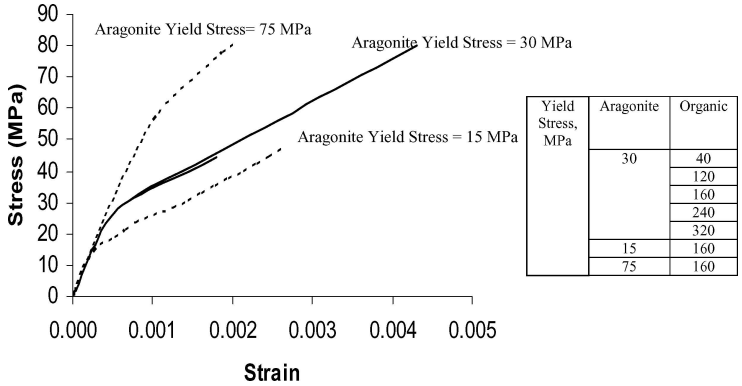


| Yield Stress, MPa | Aragonite | Organic |
|---|---|---|
| 30 | | 40 |
| | | 120 |
| | | 160 |
| | | 240 |
| | | 320 |
| 15 | | 160 |
| 75 | | 160 |

*Figure 8* Plot of Stress-Strain response of nacre from simulations for various values of yield stress of organic phase and aragonite. For a wide range of values of yield stress of organic phase and constant yield stress of aragonite, the yield stress of nacre is about the same, 28 MPa. The yield stress of nacre becomes 13 and 58 MPa when the yield stress of aragonite is assigned values of 15 and 75 MPa respectively. Since, the experimentally obtained yield stress of nacre is of the order of 50 to 60 MPa, the yield stress of aragonite in nacre is of the order of 75 MPa. The results indicate that yield stress of aragonite has the major influence on magnitude of yield stress in nacre.

of aragonite was maintained at 30 MPa and the yield stress of organic phase was varied from 320 to 40 MPa. The simulations show that for the entire range of yield stress of organic phase, the yield stress of nacre is about 28 MPa. There is very marginal difference in the yield stress of nacre over the wide range of yield stress values of the organic phase as can be seen by the overlapping curves in the figure. Next, the yield stress of the organic phase was kept constant at 160 MPa and the yield stress of the aragonite was changed to 15 and 75 MPa respectively. The yield stress of nacre obtained from the simulations is 13 and 58 MPa respectively. Since the yield stress of nacre obtained from experiments is of the order of 50 to 60 MPa [1], the yield stress of aragonite in nacre is of the order of 75 MPa.

## 4. Conclusions

A 3D finite element model representing more truly the pseudo-hexagonal symmetry of aragonite platelets in nacre has been constructed. Atomic force microscopy and nanoindentation experiments were performed to give material parameters of the organic and inorganic phases. In addition, details of nanoarchitecture of nacre including small rotations between aragonitic platelet layers and presence of mineral contacts between the layers was incorporated into the 3D models. We quantitatively analyzed the influence of the mineral contacts on the bulk mechanical response of nacre. Our simulations suggest that the contacts have marginal effect of the elastic properties of nacre. Furthermore, effective stresses in the contact regions are approximately three times higher than that applied. This suggests that the stress values at which yield starts in nacre is much higher than yield initiation of aragonite in the contact regions. In other words, the mineral contacts break long before yield initiates in nacre and thus are of minimal consequence in the yield behavior of nacre also. Our work also indicates that the magnitude of yield stress of nacre is mainly influenced by the yield stress of the aragonite. Our current simulations have assumed perfect load transfer at organic-inorganic interfaces. Our subsequent work focuses on quantifying role of nano and micro scale asperities at these interfaces on the linear and nonlinear responses in nacre.

## Acknowledgements

The authors acknowledge support from National Science Foundation (project # 0115928). The cognizant program officer is Dr. K. Chong. The authors (MS and JMS) also acknowledge support from ARO-DURINT. The author (DK) acknowledges the National Center for Supercomputer Applications for supercomputer time and software support on the Origin 2000 system.

## References

1. J. D. CURREY, in "The Mechanical Properties of Biological Materials," edited by J. F. V. Vincent and J. D. Currey (Cambridge University Press, London, 1980) p. 75.
2. A. P. JACKSON, *J. Mater. Sci. Lett.* **5** (1986) 975.
3. J. F. V. VINCENT, "Structural Biomaterial." (MacMillan Press, London, 1982) p. 171.
4. M. SARIKAYA, and I. A. AKSAY, in " Structure, Cellular Synthesis, and Assembly of Biopolymers," edited by S. Case (Springer-Verlag, Berlin, 1995) p. 1.
5. L. ADDADI and S. WEINER, *Agnew Chem. Int. Ed Engl.* **31** (1992) 153.
6. A. P. JACKSON, J. F. V. VINCENT and R. M. TURNER, *Proc. R. Soc. Lond.* **B234** (1988) 415.
7. M. YASREBI, G. H. KIM, K. E. GUNNISON, D. L. MILIUS, M. SARIKAYA and I. A. AKSAY, *Mat. Res. Soc. Proc.* **180** (1990) 625.
8. M. SARIKAYA, K. E. GUNNISON, M. YASREBI, D. L. MILIUS and I. A. AKSAY, *Mat. Res. Soc. Proc.* **174** (1990) 109.
9. K. SIMKISS and K. M. WILBUR, "Biomineralization: Cell Biology and Mineral Deposition" (Academic Press, New York, 1989) p. 231.
10. A. H. HEUER, D. J. FINK, D. J. LARAJAI, J. L. ARIAS, P. D. CALVERT, K. KENDALL, G.L. MESSING, J. BLACKWELL, P. C. RIEKE, D. H. THOMPSON, A. P. WHEELER, A. VEIS and A. I. KAPLAN, *Science* **255** (1992) 1098.
11. P. CALVERT, *Mater. Res. Soc. Symp. Proc.* **180** (1990) 619.
12. K. S. KATTI, M. QIAN, D. W. FRECH and M. SARIKAYA, *Microsc. Microanal.* **5** (1999) 358.
13. C. S. DESAI and J. F. ABEL, "Introduction to the Finite Element Method" (Van Nostrand Reinhold, New York, 1972).
14. S. E. BORGERSEN and R. L. SAKAGUCHI, *ASME Int. Mech. Eng. Conf.* **28** (1994) 129.
15. G. W. BRODLAND and D. A. CLAUSI, *J. Biomech. Eng.* **116** (1994) 146.
16. K. K. MENDIS, R. L. STALNAKER and S. H. ADVANI, *ibid.* **117** (1995) 279.
17. D. R. KATTI and K. S. KATTI, *J. Mater. Sci.* **36**(6) (2001) 1411.
18. D. R. KATTI, K. S. KATTI, J. SOPP and M. SARIKAYA, *J. Theo. Comp. Poly. Sci.* **11** (2001) 397.
19. K. S. KATTI, D. R. KATTI, J. M. SOPP, W. M. MERCER and M. SARIKAYA, in 10th International Conference on Computer Methods and Advances in Geomechanics (IACMAG), edited by Desai, Kundu, Harpalani, Contractor and Kemeny (2001) Vol. 1, p. 537.
20. W. C. OLIVER and G. M. PHARR, *J. Mater. Res.* **7**(6) (1992) 1564.

*Received 16 December 2002*
*and accepted 19 October 2004*